JOURNAL OF MATERIALS SCIENCE 18 (1983) 2618–2628

Fracture of metastable tetragonal zirconia crystals

D. MICHEL, L. MAZEROLLES, M. PEREZ Y JORBA
Laboratoire de Chimie Appliquée de l'Etat Solide, LA 302, CECM 15 rue Georges Urbain, 94400 Vitry sur Seine, France

Crystals of single-phased metastable tetragonal zirconia (MTZ) were prepared from skull-melting at the composition ZrO_2–3 mol % M_2O_3 (M = Y, Yb or Gd). The fracture of the tetragonal crystals occurred differently than for the cubic stabilized zirconia ones. The toughness was much higher for the tetragonal specimens and the cleavage planes were not the same as for the fluorite crystals. The results were interpreted by considering the domain microstructure induced by the cubic → tetragonal phase transformation undergone by the crystals.

1. Introduction

Recent studies have revealed remarkable mechanical properties for materials based on zirconium dioxide and this has led to a considerable interest in the field of "partially stabilized zirconia" (PSZ) [1–27].

High values were reported for both strength (500 to 1000 MPa) and fracture toughness (K_{Ic} = 5 to 10 MN $m^{-3/2}$).

A decrease in the brittleness occurs in zirconia ceramics when a small amount of an alloying agent (MgO, CaO, Y_2O_3, etc.) is added to ZrO_2. Maximum values of fracture toughness are obtained in the composition range 94 to 98 mol % ZrO_2 for samples in which "metastable tetragonal zirconia" (MTZ) is the major constituent phase and toughening agent.

At atmospheric pressure, pure zirconium dioxide possesses three crystallographic forms: monoclinic ($P2_1/c$, $Z = 4$) at low temperature, tetragonal ($P4_2/nmc$, $Z = 2$) stable between 1100 and 2400° C and cubic ($Fm3m$, $Z = 4$) at high temperature.

The monoclinic and tetragonal forms are distorted modifications of the cubic structure of the fluorite-type.

The tetragonal phase cannot be retained at room temperature for pure ZrO_2 by quenching because of the diffusionless martensitic transition into monoclinic zirconia. The addition of a stabilizing oxide lowers the transition temperatures monoclinic ⇄ tetragonal ⇄ cubic and favours the retention of tetragonal and cubic zirconia at room temperature.

Single-phased tetragonal samples are only obtained in well-defined preparative conditions [9, 10, 20, 22, 23, 28–30]. As discussed in recent papers [9, 10, 20, 22, 23], the retention of tetragonal zirconia is dependent on factors such as density, composition, grain size and firing treatments.

Zirconia ceramics with a low additional content (for instance 2 to 9 mol % MgO, CaO or Y_2O_3) prepared by solid state reaction generally consist of two (or three) phases, depending on the above-mentioned factors.

Monoclinic or tetragonal zirconia are obtained as coherent precipitates in a tetragonal or cubic zirconia matrix because of the crystallographic relationships between the different phases.

Mechanical properties have been extensively studied on PSZ sintered ceramics and are strongly influenced by the nature and distribution of the constituent phases. For instance, microstructural developments during ageing induces important modifications in the fracture toughness [17, 18]. Different mechanisms have been proposed and discussed to explain the enhanced mechanical properties of PSZ [5, 8, 11–13, 15, 23, 31–36].

One of the important toughening mechanisms, elucidated by Porter *et al.* [8, 11, 12] is the

0022–2461/83 $03.00 + .12

stress-induced transformation of the metastable tetragonal phase in the vicinity of a crack into the monoclinic stable variety.

The monoclinic transformed zone was detected by different techniques: electron microscopy [8, 11, 12, 17, 19], Raman microprobe analysis ahead of crack propagation [37], X-ray analysis on fracture surfaces [38, 39]. The depth of the transformed zone measured on different PSZ lies in the range 0.5 to 5 μm.

The enhancement in fracture toughness has been related for these materials to the fraction of retained metastable tetragonal phase and the depth of the transformed zone, in agreement with theoretical arguments [23].

The present paper is concerned with the intrinsic toughness of crystals of metastable tetragonal zirconia (MTZ) prepared by solidification from the melt.

For crystals in which the stabilization of the tetragonal phase is achieved by sufficient quenching conditions, phase transformation into monoclinic zirconia cannot account for their high fracture toughness.

In spite of studies by different techniques (electron microscopy, Raman microscopy and X-ray analysis on fracture surfaces) to reveal an eventual transformed zone, the results indicated the absence of a measurable amount of monoclinic zirconia.

Recent work by Ingel *et al.* [27] on crystals obtained by a similar technique shows that the greater strength and toughness of PSZ crystals relative to cubic zirconia is maintained above the monoclinic → tetragonal transformation temperature. This result demonstrates that mechanisms other than phase transformation toughening must be operative in materials prepared from high-temperature processes.

Structural and microstructural studies were performed on large MTZ crystals grown from skull-melting with the conditions of composition and quenching leading to single-phased samples of tetragonal zirconia.

Fluorite-type cubic single crystals are elaborated from the melt, but because of the cubic → tetragonal transition undergone at about 2000° C, microtwinned crystals were obtained at room temperature. Their domain microstructure was studied by transmission electron microscopy in relation with symmetry considerations on the phase transition.

The fracture toughness of polydomain tetragonal samples (ZrO_2–3 mol% M_2O_3, M = Y, Gd or Yb) was much higher than that of monodomain cubic zirconia ones (ZrO_2–9 mol% M_2O_3).

Observations on fracture surfaces showed that the fracture occurred along different crystallographic planes for cubic and tetragonal zirconia crystals.

The fracture mode and the toughness of MTZ crystals are interpreted considering:

1. their domain microstructure and the internal stresses resulting from the cubic → tetragonal transition

2. the differences between the fluorite structure and its tetragonally distorted variety.

2. Experimental details

2.1. Preparation of MTZ crystals

The starting materials were high-purity ZrO_2 (99.9 Ugine Kuhlman) and yttrium, ytterbium or gadolinium sesquioxide (Rhône Poulenc 3N) powders.

The elaboration of tetragonal zirconia crystals was reported in a previous paper on the crystal growth of fluorite-related phases in ZrO_2–Ln_2O_3 systems [40]. Crystals are grown by directional solidification after r.f. induction melting according to the skull-melting technique developed in our Laboratory [41–44].

Growth runs were performed at different compositions and with different solidification rates. Best conditions for the obtention of samples consisting only of tetragonal zirconia are for the 3 mol% M_2O_3 composition with a sufficiently rapid cooling process ($> 400° h^{-1}$). These results are in good agreement with the experimental conditions determined by Lefevre [29] for the retention of the tetragonal phase. The average size of the crystals obtained from a 500 g melt is 15 mm × 5 mm × 5 mm.

With lower cooling rates or with an addition of sesquioxide lower than 3 mol%, monoclinic zirconia is present in addition to the tetragonal phase. Mixtures of tetragonal and cubic phases are obtained with similar experimental conditions when the sesquioxide amount exceeds 5 mol%.

The analysis of constituent phases was determined from X-ray powder diffractometry on ground crystals. The amount of each phase can be estimated from the relative intensity of diffraction lines. The proportion of monoclinic zirconia was

determined from the intensity of 111 and $11\bar{1}$ monoclinic and 111 tetragonal lines.

Tetragonal samples obtained in the above-mentioned conditions are free of the monoclinic phase and cannot be easily transformed by grinding or polishing. Long-continued milling treatments are required to obtain a fraction of monoclinic zirconia that is detectable by X-ray powder diffraction (about 0.5%). For instance, the milling of crystals to a grain size of 1 micron induces only the transformation of less than 1% of the tetragonal phase into monoclinic zirconia.

2.2. Structure determination

The structure of a yttrium MTZ phase was refined from the powder diagram ($CoK\alpha$) ranging from 0 to 66° Bragg angles. The line intensities were measured for 25 independent reflections and corrected by Lorentz-polarization factors. A least squares refinement was undertaken with the z-variable position parameter of oxygen atoms and with the isotropic Debye–Waller factors for oxygen and zirconium (or yttrium) atoms.

The atomic positions are those as determined by Teufer [45] for a high temperature tetragonal zirconia, and a random distribution of anionic vacancies and of substitutional yttrium atoms is assumed in the studied compound $(Zr_{0.94}Y_{0.06})O_{1.97}$. Scattering factors for the ions Zr^{4+} and O^{2-} were taken from Cromer and Waber [46] (Zr^{4+} and Y^{3+} being isoelectronic the substitution of yttrium to zirconium has a negligible influence on the cation scattering factor).

2.3. Electron microscopy

From the MTZ single phased crystals, platelets were oriented and thinned for transmission electron microscopy (TEM) observations on a Jeol 200 CX. Thinning was achieved by a mechanical polishing followed by argon ionic bombardment.

2.4. Fracture

The polydomain crystals were broken by applying mechanical stress or shocks. Cleavage orientations were determined from Laue patterns and the fracture surfaces were observed by scanning electron microscopy (SEM) after gold metallization.

The fracture toughness was estimated from the size of cracks produced by Vickers indentation with a Leitz Microdurimet (loads from 100 to 2000 g) on polished oriented specimens.

3. Results and discussion

3.1. Structure of tetragonal zirconia stabilized at room temperature

For the tetragonal phases retained at room temperature, the following unit-cell parameters were determined:

$$ZrO_2\text{–}3\,\text{mol}\%\,Yb_2O_3,\quad a = 0.3605\,\text{nm},$$
$$c = 0.5166\,\text{nm},\quad c/a(2)^{1/2} = 1.013;$$
$$ZrO_2\text{–}3\,\text{mol}\%\,Y_2O_3,\quad a = 0.3610\,\text{nm},$$
$$c = 0.5168\,\text{nm},\quad c/a(2)^{1/2} = 1.012;$$
$$ZrO_2\text{–}3\,\text{mol}\%\,Gd_2O_3,\quad a = 0.3614\,\text{nm},$$
$$c = 0.5174\,\text{nm},\quad c/a(2)^{1/2} = 1.013.$$

Results of the structure determination for the yttria-stabilized phase are given in Table I. The refinement was undertaken on the average atomic positions, the relaxations of atoms surrounding anionic vacancies (1.5% of available sites) not being taken into account. The final computing step provides an agreement factor $R = 0.045$.

The tetragonal structure is derived from fluorite by the elongation of the cubic lattice along the 4-fold axis and by slight shifts from oxygen fluorite positions.

Tetragonal unit-cell vectors $\mathbf{a}_t, \mathbf{b}_t, \mathbf{c}_t$ are related as follows by ϵ to the parameter a_c of the corresponding fluorite (with a same unit-cell volume):

$$\mathbf{a}_t = (\mathbf{a}_c + \mathbf{b}_c)(1-\epsilon)/2$$
$$\mathbf{b}_t = (\mathbf{b}_c - \mathbf{a}_c)(1-\epsilon)/2$$
$$\mathbf{c}_t = \mathbf{c}_c(1+2\epsilon)$$

The tetragonal distortion of the fluorite lattice is measured by the value of ϵ with $\epsilon \simeq 4 \times 10^{-3}$ for the considered phases stabilized at room temperature. For pure ZrO_2, a higher deformation $\epsilon \simeq 8 \times 10^{-3}$ was measured in the tetragonal stability range between 1160 to 2165° C [45, 47, 48].

On Fig. 1a, tetragonal nodes for the primitive lattice are represented by full circles. The $\frac{1}{2}\frac{1}{2}\frac{1}{2}$ position (empty circle) corresponds to an equivalent node for the fcc fluorite lattice. The two positions are differentiated in tetragonal zirconia and are occupied by zirconium (or yttrium) atoms surrounded by oxygen atoms defining a same coordination polyhedron but with a different orientation for 000 and $\frac{1}{2}\frac{1}{2}\frac{1}{2}$ as shown on Fig. 1b.

A displacement vector $(0.25 - z)\,\mathbf{c}_t$ (z being

TABLE I Structural data concerning tetragonal zirconia (stabilized by 3 mol % Y_2O_3). Comparison with a MO_2 fluorite structure with same unit-cell volume

	Tetragonal $Zr_{1.94}Y_{0.06}O_{1.97}$	Corresponding fluorite MO_2
Space group	$P4_{2/n}mc$, $Z = 2$	$Fm3m$, $Z = 4$
Parameters	$a_t = 0.3610$ nm; $c_t = 0.5168$ nm	$a_c = 0.5126$ nm
Atomic positions	2(a) Zr (or Y) 000 $B = 0.002$ nm^2 4(d) O (or vacancy) $0\frac{1}{2}z$ $z = 0.199$ $B = 0.025$ nm^2	$z = 0.250$
Cation environment	4 Zr–O 0.208 nm 4 Zr–O 0.238 nm 4 Zr–Zr 0.361 nm 8 Zr–Zr 0.363 nm	8 M–O 0.222 nm 12 M–M 0.362 nm
Anion environment	2 O–Zr 0.208 nm 2 O–Zr 0.238 nm 2 O–O 0.258 nm 4 O–O 0.261 nm	4 O–M 0.222 nm 6 O–O 0.256 nm

the variable position parameter for the oxygen atoms) defines the shift of the oxygen atom positions from ideal fluorite ones. This displacement (0.026 nm for (Zr, Y) $O_{1.97}$) induces the distortion from a cubic symmetry of the cation coordination polyhedra (Fig. 1b).

In the room-temperature structure of (Zr, Y)$O_{1.97}$ cations are surrounded by two sets of 4 oxygen atoms at, respectively, 0.208 and 0.238 nm. Very similar polyhedra are found in the high-temperature ZrO_2 variety. Metal–oxygen distances are 0.207 to 0.209 nm and 0.244 to 0.247 nm between 1200 and 2045° C [48].

3.2. Microdomain structure induced by the cubic → tetragonal transition

For pure zirconium dioxide, a tetragonal ⇄ cubic phase transition was reported above 2300° C at a temperature depending on the oxygen partial pressure [48–51].

This transition is according to the classification of Aizu [52] of para ⇄ ferroelastic type (m3m $F4/m$ mm).

In the ZrO_2-rich portion of phase diagrams between zirconia and a stabilizing oxide (i.e. Y_2O_3), the existence of domains of the cubic and tetragonal phases are separated by a two-phased (c + t) region [30, 51, 53]. By high-temperature X-ray diffraction and thermal analysis, Rouanet determined the temperature T_c above which the single-phased cubic solid solution is stable [51]. At the considered composition (3 mol % M_2O_3) values are T_c = 1950° C (Yb_2O_3), T_c = 2000° C (Y_2O_3) and T_c 2050° C (Gd_2O_3).

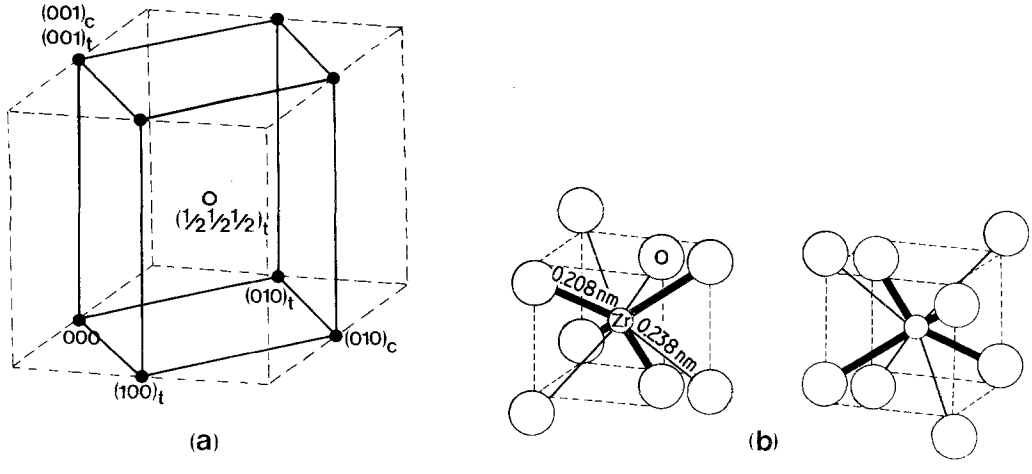

Figure 1 Relationships between the tetragonal and fluorite structures (a) Correspondence between the lattices (b) Environment of cations occupying 0 0 0 (left) and $\frac{1}{2}\frac{1}{2}\frac{1}{2}$ (right) positions in $Zr_{0.94}Y_{0.06}O_{1.97}$.

The crystals grown from the melt are first solidified with the cubic fluorite-type structure and are transformed subsequently to display the tetragonal symmetry below T_c.

Because of this transformation, the obtained crystals must present a domain microstructure. The number of orientation states and the crystallographic relationships between domains are ruled by the symmetry of both prototype and ferroelastic phases [52]. They are given by the decomposition of the high symmetry space group G into co-sets with respect to its low-temperature phase subgroup H [54].

For the cubic → tetragonal transition, this decomposition will admit 6 translation/orientation operators (Seitz notation):

$$G = (1,000)H + (3^1,000)H + (3^2,000)H + (1,\tfrac{1}{2}\tfrac{1}{2}\tfrac{1}{2})H + (3^1,\tfrac{1}{2}\tfrac{1}{2}\tfrac{1}{2})H + (3^2,\tfrac{1}{2}\tfrac{1}{2}\tfrac{1}{2})H$$

with

$$G = Fm3m\ (\mathbf{a_c} = \mathbf{a_t} - \mathbf{b_t}, \mathbf{b_c} = \mathbf{a_t} + \mathbf{b_t}, \mathbf{c_c} = \mathbf{c_t})$$

$$H = P4_2/nmc\ (\mathbf{a_t}, \mathbf{b_t}, \mathbf{c_t}).$$

The 6 variants are equiprobable and correspond to three different orientations for the 4-fold axis combined with one antiphase possibility ($\frac{1}{2}\frac{1}{2}\frac{1}{2}$ translation).

The expected domain microstructure was confirmed by TEM examinations on oriented platelets. Crystals were thinned with the $\{001\}_c$ and $\{110\}_c$ orientations for which tetragonal axes are in the observation plane.

Platelets with $\{001\}_c$ orientation display either the $\mathbf{a_t}$ and $\mathbf{b_t}$ tetragonal axes or the $\mathbf{c_t}$ axis depending on the variant. On the dark field micrograph (Fig. 2a) obtained with a 110 spot, bright

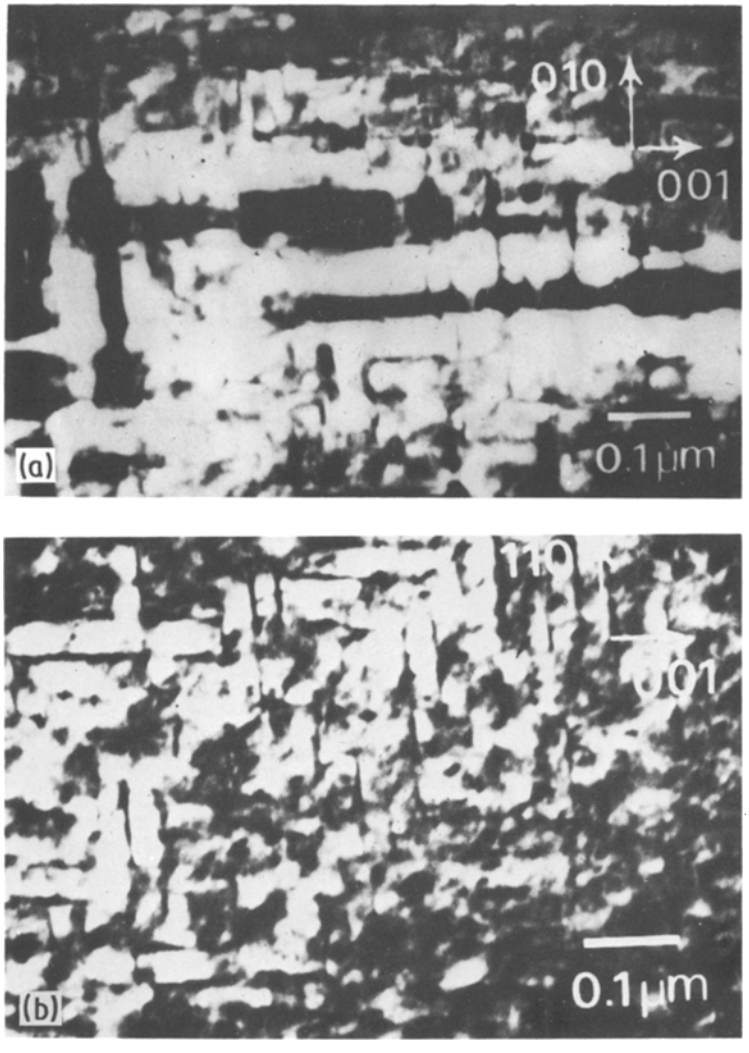

Figure 2 Domain microstructure of MTZ crystals observed by transmission electron microscopy (dark-field) (a) oriented {0 0 1} crystal platelet. Diffraction spot 1 1 0 (b) Oriented {1 1 0} crystal platelet. Diffraction spot 1 1 2. The indexation is referred to the cubic fluorite axes.

domains correspond to the orientation states with the tetragonal axis parallel to the electron beam. For the $\{1\,1\,0\}_c$ orientation, bright domains have the 4-fold axis parallel to the observation plane (Fig. 2b). Antiphase boundaries appear as inverse lines between two domains in the same orientation state with the same contrast.

Domains are elongated along $\langle 0\,0\,1\rangle$ directions with habit planes $\{0\,0\,1\}$; their mean size is about 50 nm. Our results are in good agreement with the previous observations of Scott [30] and Garvie *et al.* [4] and Hanninck [55] on MTZ powders.

3.3. Fracture study of MTZ crystals

Hardness and fracture toughness of MTZ crystals were compared to that of fully stabilized cubic ones (ZrO_2–9 mol% Y_2O_3) prepared by the same technique.

An appreciable anisotropy in hardness was observed from Knoop indentation for both materials, but for a given crystallographic orientation cubic and tetragonal zirconia possess roughly the same hardness. Values measured on the $\{0\,0\,1\}$ and $\{1\,1\,0\}$ fluorite-type planes are ranging from 11.9 to 14.9 GPa for the cubic crystals (9 mol% Y_2O_3) and from 11.5 to 13.5 GPa for tetragonal ones (3 mol% Y_2O_3) [56].

On the contrary, a very different behaviour was observed for the crystal fracture with a much higher toughness for tetragonal samples.

3.3.1. Fracture toughness

Cubic zirconia crystals are significantly more brittle than the tetragonal ones. Cracks are produced easily by Vickers indentation with only a 100 g load on $\{0\,0\,1\}$ planes. No fissures appear on the tetragonal crystals with loads lower than 1500 g for the same orientation.

Observations of indentation on various crystallographic planes demonstrated that crack initiation on tetragonal crystal requires at least loads ten times higher than for cubic crystals.

Measurements of the ratio of the crack length to the indent size for different orientations and different loads provided estimation of fracture toughness using the calibration curve developed by Evans and Charles [57].

The following average values (deviation ±30%) calculated for critical stress-intensity factors are comparable to that reported for polycrystalline [9, 15] or single crystal [26, 27] specimens $K_C = 1.8\,MN\,m^{-3/2}$ for the cubic phase 9 mol% Y_2O_3 and $K_C = 6\,MN\,m^{-3/2}$ for the tetragonal phase 3 mol% Y_2O_3.

3.3.2. Fractographic study of cubic and tetragonal zirconia crystals

The crystal fracture was found to occur by cleavage on different planes for cubic and tetragonal zirconia. Cubic zirconia crystals were cleaved along $\{1\,1\,1\}$ planes exhibiting large mirrors. This fracture produces the breaking of a minimal number of anion–cation bonds per surface area (4 bonds per $0.61\,a_c^2$) and is the usual cleavage of crystals with the CaF_2 structure.

In spite of their structural relationship with the fluorite-type, MTZ crystals are not cleaved along planes corresponding to $\{1\,1\,1\}_c$ cubic ones but to $\{0\,0\,1\}_c$ planes.

Fig. 3 shows the X-ray diffractional pattern of a fracture surface of a tetragonal zirconia crystal. Only the lines deriving from the $\{0\,0\,1\}$ fluorite

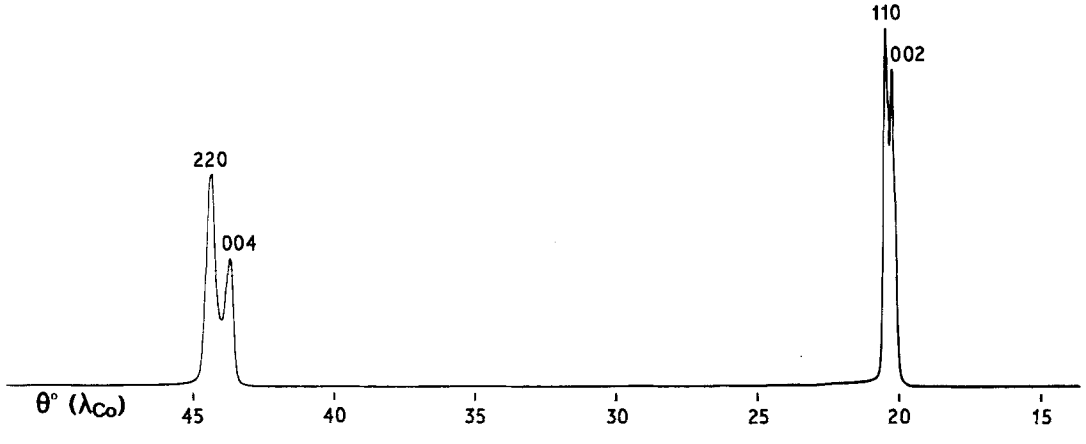

Figure 3 MTZ crystal (ZrO_2–3 mol% Y_2O_3) X-ray diffraction pattern obtained on the fracture surface (cobalt anticathode).

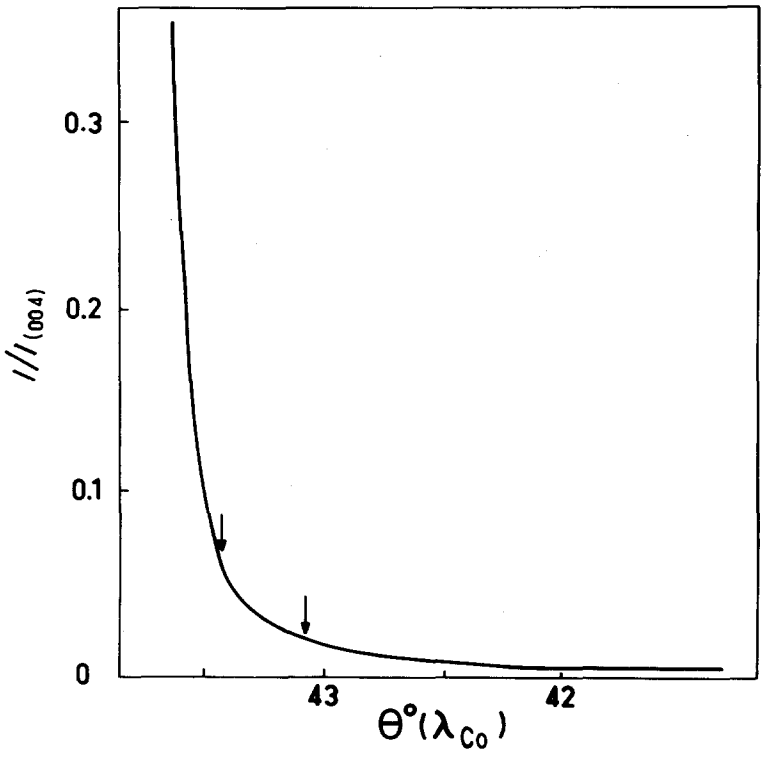

Figure 4 MTZ crystal (ZrO_2–3 mol% Y_2O_3) X-ray diffracted intensity in the range 42 to 44°θ showing the absence of monoclinic zirconia reflections (positions indicated by arrows) – cobalt anticathode.

orientation are obtained. Other interferences are affected by a complete extinction.

The splitting of 0 0 2 and 0 0 4 fluorite lines indicates that variants with the different possible orientations of the 4-fold axis are involved in the crystal fracture.

Intensity countings demonstrate the absence of a detectable amount of monoclinic zirconia on the fracture surface of MTZ crystals. The diffracted intensity recorded in the range 42 to 44°θ (cobalt anticathode) is reported in Fig. 4. The 0 0 4 and 0 4 0 monoclinic lines would be observed in addition to the 0 0 4 tetragonal peak (at positions indicated by arrows) if the surface contained transformed monoclinic zirconia. Very strong tetragonal peaks were obtained on oriented surfaces. For the 0 0 4 tetragonal line, the signal/noise ratio was about 500 with a variation in the background noise of less than ± 10%. In these conditions, the threshold for the detection of monoclinic zirconia can be estimated to about 0.2%.

For the used wavelength ($\lambda_{K\alpha} = 0.17889$ nm), the absorption coefficients are, respectively, 0.0960 μm^{-1} for monoclinic zirconia and 0.0994 μm^{-1} for tetragonal zirconia. Therefore, at the considered Bragg angles, a transformed monoclinic zone on the fracture surface with a depth higher than 0.01 μm would give rise to observable 0 0 4 and 0 4 0 monoclinic lines.

Raman spectroscopy measurements confirmed the purity of the tetragonal phase on the fracture surface. Monoclinic and tetragonal zirconia can be characterized from their Raman spectra which are quite different [58–61]. The spectrum of MTZ crystals consists only of the 6 Raman lines allowed by symmetry [60]. For mixtures of monoclinic and tetragonal zirconia, additional lines are obtained especially at 179 and 191 cm^{-1} where the two strongest lines of monoclinic zirconia are located [37]. Raman spectra were obtained on fracture surfaces of tetragonal crystals with a low incidence for the laser beam. As shown in Fig. 5 only the tetragonal phase was found. Countings at 179 and 191 cm^{-1} verified the absence of monoclinic zirconia.

These results and observations by TEM with various magnifications [62] indicate that monoclinic zirconia is not involved in the toughening process for the considered tetragonal crystals. Toughening relative to single crystals of cubic zirconia has to be related to the different fracture mode induced by the domain microstructure in tetragonal zirconia crystals.

Fracture surfaces of MTZ crystals exhibit a very roughened aspect. A similar roughness was

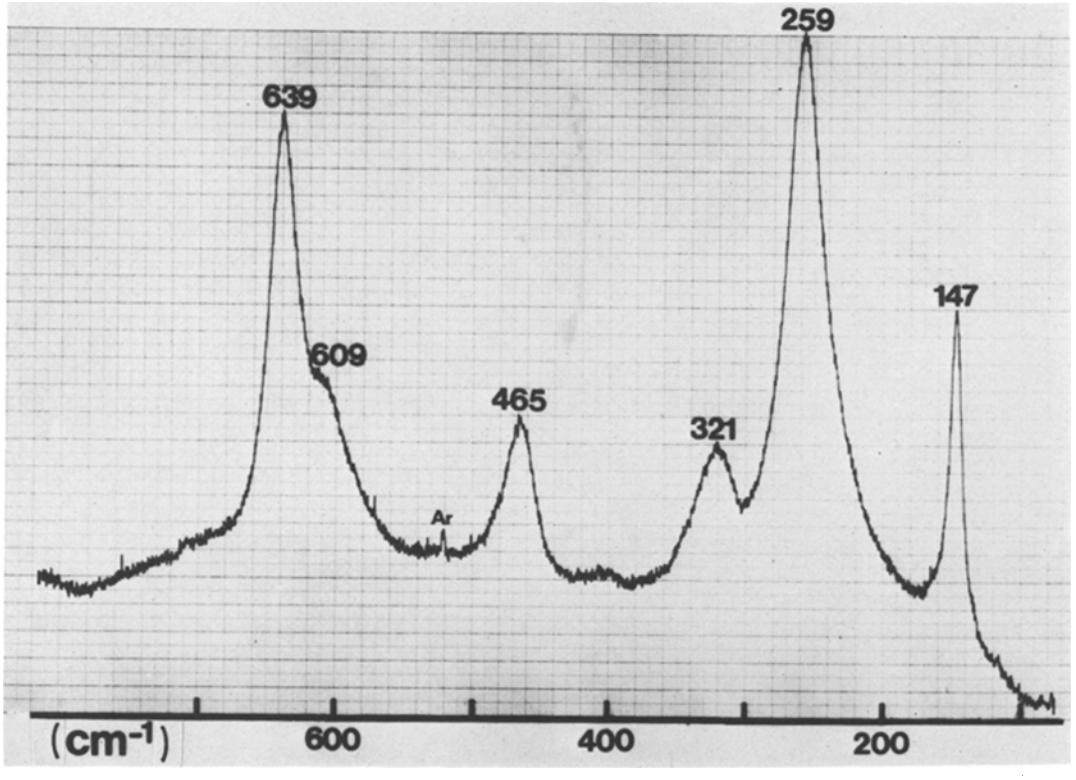

Figure 5 MTZ crystal (ZrO_2–3 mol% Y_2O_3) Raman spectrum of a fracture surface (laser beam with a low incidence angle). Argon wavelength $\lambda = 514.5$ nm.

obtained by Ingel *et al.* [27] on the fracture surface of a ZrO_2–5 wt% Y_2O_3 crystal fractured at 1500° C above the monoclinic → tetragonal transition.

Our examinations by scanning electron microscopy on fracture surfaces previously referenced from their Laüe pattern, indicate that cleavage occurs along planes corresponding to $\{0\,0\,1\}_c$ fluorite. Faceted kinks are produced by fracture with $\{0\,0\,1\}_c$ faces as shown on Fig. 6. Kinks have about the same dimensions (50 nm) as those of the microdomains observed by transmission electron microscopy.

3.3.3. Proposed fracture mechanism: relation with toughening

The fracture topography of MTZ crystals demonstrates changes in directions of crack propagation following the three $\{0\,0\,1\}$ axes of the related-fluorite. This fracture mode may be interpreted by changes of 90° for the easy-cleavage plane from one domain to another in a different orientation state. The plane of easier cleavage is either $\{0\,0\,1\}_t$ or $\{1\,1\,0\}_t$ which are the orientation of fracture surfaces.

From structural considerations, it is likely that the preferred cleavage occurs along $\{0\,0\,1\}_t$ planes normal to the 4-fold axis.

The main difference with the fluorite structure lies in the presence of two types of metal–oxygen bonds in the tetragonal zirconia. Very different bond strengths can be associated to the two M–O bonds with 0.208 and 0.238 nm. Using the empirical relations developed by Zachariasen [63], the bond strength, s, calculated for shorter M–O bonds is $s = 0.72$ whereas $s = 0.30$ for longer ones.

As shown in Fig. 7, cleavage perpendicular to the 4-fold axis produces the breaking of more M–O bonds (4 bonds for a_c^2) than $\{1\,1\,1\}_c$ cleavage, but in this fracture mode only the longer M–O bonds are broken without involving the stronger M–O bonds (0.208 nm) represented by heavy lines. On the contrary, cleavage along any plane other than $\{0\,0\,1\}_t$ would require broken bonds with 0.208 and 0.238 nm length.

In conclusion, the cubic → tetragonal transition undergone during the preparation from the melt of tetragonal zirconia crystals seems to be responsible for the high fracture toughness of these materials.

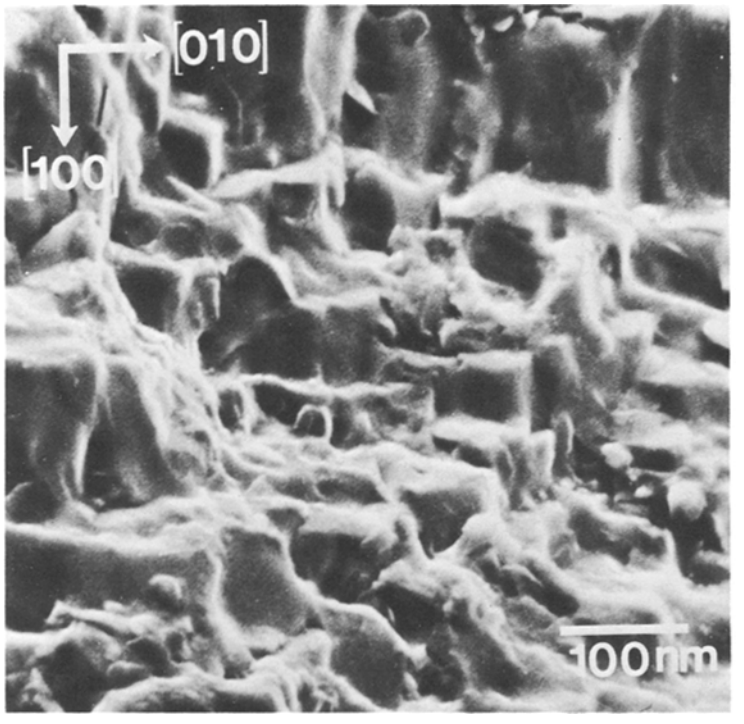

Figure 6 MTZ crystal (ZrO_2–3 mol% Y_2O_3) scanning electron micrograph on the {0 0 1} fracture surface. Indexation with reference to the fluorite directions.

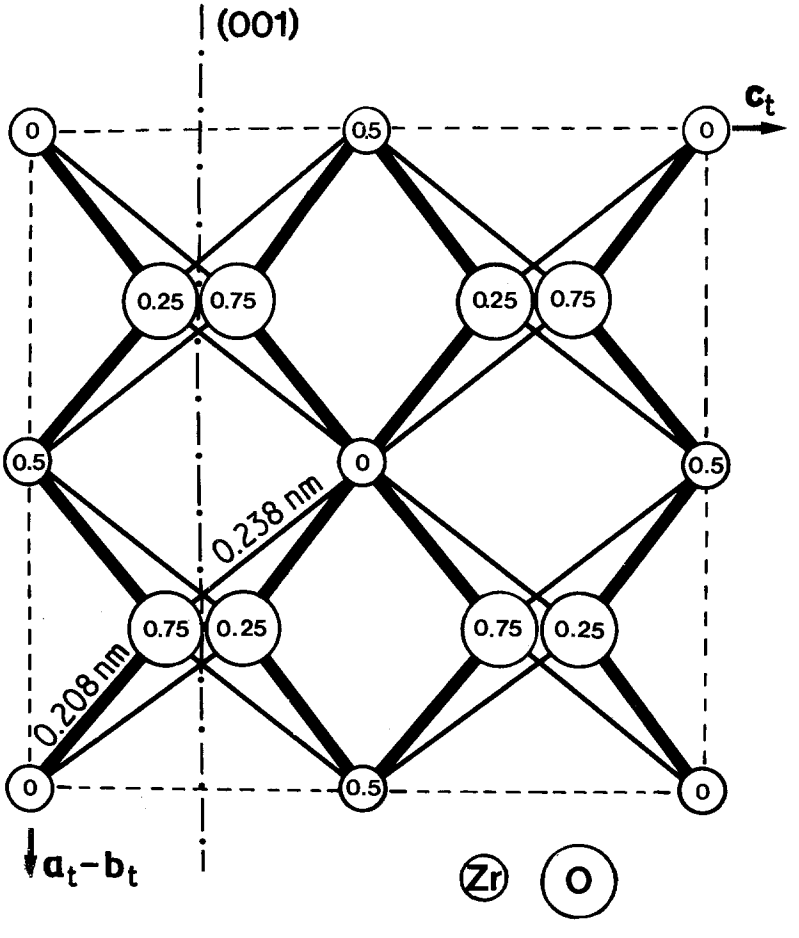

Figure 7 Cleavage model for tetragonal zirconia crystals. $(1\,1\,0)_t$ projection of the tetragonal structure, the chain dotted line represents cleavage along $(0\,0\,1)_t$.

The observed changes in {0 0 1} cleavage directions impeding crack propagation can be interpreted by the microstructure in elongated domains with {0 0 1} habit planes induced by this transition.

In addition, internal stresses resulting from the tetragonal lattice distortion are another factor favouring crack pinning at domain boundaries as pointed out by Rice *et al.* [36].

The following parameters are involved in the proposed toughening mechanism:

1. the ϵ value defining the spontaneous strain produced by the cubic → tetragonal lattice deformation

2. the displacement vectors from fluorite anionic positions which give rise to two kinds of metal–oxygen bonds and can explain the observed {0 0 1} cleavage

3. the size and morphology of domains.

The two first factors are determined by the structure of the tetragonal zirconia and depend on the nature and the composition of the oxide alloying ZrO_2. The microstructural features are influenced in addition by preparative conditions and especially by thermal treatments.

Acknowledgements

The authors wish to thank A. Kahn (ENSCP, Paris) for structure refinement, C. Haud (Laboratoire de Métallurgie, Orsay) for SEM observations, J. Rzepski and R. Portier (CECM, Vitry) for TEM observations.

References

1. A. G. KING and P. J. YAVORSKY, *J. Amer. Ceram. Soc.* **51** (1968) 38.
2. R. GARVIE and P. S. NICHOLSON, *ibid.* **55** (1972) 152.
3. D. J. GREEN, P. S. NICHOLSON and J. D. EMBURY, *ibid.* **55** (1973) 619.
4. R. C. GARVIE, R. H. HANNINCK and R. T. PASCOE, *Nature* **258** (1975) 703.
5. G. K. BANSAL and A. H. HEUER, *J. Amer. Ceram. Soc.* **58** (1975) 235.
6. N. CLAUSSEN, R. F. PABST and C. P. LAHMANN, *Proc. Brit. Ceram. Soc.* **25** (1975) 139.
7. R. C. GARVIE, R. H. HANNINCK, R. R. HUGHAN, N. A. McKINNON, R. T. PASCOE and R. K. STRINGER, *J. Aust. Ceram. Soc.* **13** (1977) 8.
8. D. L. PORTER and A. H. HEUER, *J. Amer. Ceram. Soc.* **60** (1977) 183.
9. T. K. GUPTA, J. H. BECHTOLD, R. C. KUZNICKI, L. H. CADOFF and B. R. ROSSING, *J. Mater. Sci.* **12** (1977) 2421.
10. T. K. GUPTA, F. F. LANGE and J. H. BECHTOLD, *ibid.* **13** (1978) 1464.
11. D. L. PORTER, A. G. EVANS and A. H. HEUER, *Acta Metall.* **27** (1979) 1649.
12. D. L. PORTER and A. H. HEUER, *J. Amer. Ceram. Soc.* **62** (1979) 298.
13. A. G. EVANS and A. H. HEUER, *ibid.* **63** (1980) 241.
14. R. W. RICE, K. R. McKINNEY and R. P. INGEL, *ibid.* **64** (1981) C-175.
15. H. P. KIRCHNER, R. M. GRUVER, M. V. SWAIN and R. C. GARVIE, *ibid.* **64** (1981) 529.
16. E. C. SUBBARAO, in "Advances in Ceramics" Vol. 3, edited by A. H. Heuer and L. W. Hobbs (American Ceramic Society, Columbus, 1981) p. 1.
17. A. H. HEUER, *ibid.* p. 98.
18. R. H. HANNINCK, K. A. JOHNSTON, R. T. PASCOE and R. C. GARVIE, *ibid.* p. 116.
19. N. CLAUSSEN and M. RUHLE, *ibid.* p. 137.
20. C. A. ANDERSSON and T. K. GUPTA, *ibid.* p. 184.
21. A. G. EVANS, D. B. MARSHALL and N. H. BURLINGAME, *ibid.* p. 202.
22. F. F. LANGE and D. J. GREEN, *ibid.* p. 217.
23. F. F. LANGE, *J. Mater. Sci.* **17** (1982) 225.
24. *Idem, ibid.* **17** (1982) 235.
25. *Idem, ibid.* **17** (1982) 255.
26. R. P. INGEL, R. W. RICE and D. LEWIS, *J. Amer. Ceram. Soc.* **65** (1982) C-108.
27. R. P. INGEL, D. LEWIS, B. A. BENDER and R. W. RICE, *ibid.* **65** (1982) C-150.
28. J. LEFEVRE, R. COLLONGUES and M. PEREZ Y JORBA, *CR Acad. Sci.* **249** (1959) 2329.
29. J. LEFEVRE, *Ann. Chim.* 8 (1963) 117.
30. H. G. SCOTT, *J. Mater. Sci.* **10** (1975) 1527.
31. N. CLAUSSEN, *J. Amer. Ceram. Soc.* **59** (1976) 179.
32. R. W. RICE, *ibid.* **60** (1977) 280.
33. D. L. PORTER, G. K. BANSAL and A. H. HEUER, *ibid.* **60** (1976) 179.
34. D. L. PORTER and A. H. HEUER, *ibid.* **60** (1977) 280.
35. A. G. EVANS, N. BURLINGAME, M. DRORY and W. M. KRIVEN, *Acta Metall.* **29** (1981) 447.
36. R. W. RICE, R. C. POHANKA and W. J. McDONOUGH, *J. Amer. Ceram. Soc.* **63** (1980) 703.
37. D. R. CLARKE and F. ADAR, *ibid.* **65** (1982) 284.
38. T. KOSMAC, R. WAGNER and N. CLAUSSEN, *ibid.* **64** (1981) C72.
39. R. C. GARVIE, R. H. J. HANNINCK and M. V. SWAIN, *J. Mater. Sci. Lett.* **1** (1982) 437.
40. D. MICHEL, M. PEREZ Y JORBA and R. COLLONGUES, *J. Cryst. Growth* **43** (1978) 546.
41. M. PEREZ Y JORBA and R. COLLONGUES, *CR Acad. Sci.* **257** (1963) 1091.
42. *Idem, Rev. Htes Temp. Réfract.* **1** (1964) 21.
43. D. MICHEL, M. PEREZ Y JORBA and R. COLLONGUES, *CR Acad. Sci.* **266** (1968) 1602.
44. D. MICHEL, *Rev. Int. Htes Temp. Réfract.* **9** (1972) 225.
45. C. TEUFER, *Acta Cryst.* **15** (1962) 1187.
46. D. T. CROMER and J. T. WABER, "International Tables for X-ray Crystallography" Vol. IV (Kynoch Press, Birmingham, 1974).
47. W. W. BARKER, F. P. BAILEY and W. GARRETT, *J. Solid State Chem.* 7 (1973) 448.

48. P. ALDEBERT, Thesis, Toulouse (1980).
49. D. K. SMITH and C. F. CLINE, *J. Amer. Ceram. Soc.* 45 (1962) 419.
50. A. REVCOLEVSCHI, J. HUBERT and R. COLLONGUES, *CR Acad. Sci.* 269 (1969) 265.
51. A. ROUANET, *Rev. Int. Htes Temp. Réfract.* 8 (1971) 161.
52. K. AIZU, *Phys. Rev. B* 2 (1970) 754.
53. K. K. SRIVASTAVA, R. N. PATIL, C. B. CHANDRY, K. GOKHALE and E. C. SUBBARAO, *Trans. Brit. Ceram. Soc.* 73 (1974) 85.
54. M. GUYMONT, D. GRATIAS, R. PORTIER and M. FAYARD, *Phys. Status Solidi* A38 (1976) 629.
55. R. H. J. HANNINCK, *J. Mater. Sci.* 13 (1978) 2487.
56. D. MICHEL, L. MAZEROLLES and A. M. LEJUS, to be published.
57. A. G. EVANS and E. A. CHARLES, *J. Amer. Ceram. Soc.* 59 (1976) 371.
58. C. M. PHILLIPPI and K. S. MAZDIYASNI, *ibid.* 54 (1871) 254.
59. V. G. KERAMIDAS and W. B. WHITE, *ibid.* 57 (1974) 22.
60. D. MICHEL, M. PEREZ Y JORBA and R. COLLONGUES, *J. Raman Spectrosc.* 5 (1976) 163.
61. M. ISHIGAME and T. SAKURAI, *J. Amer. Ceram. Soc.* 60 (1977) 367.
62. D. MICHEL, L. MAZEROLLES and R. PORTIER, in "Studies in Inorganic Chemistry", Vol. 3, edited by R. Metselaan, H. J. M. Heijligers and J. Schoonman (Elsevier, Amsterdam, 1983) p. 809.
63. W. H. ZACHARIASEN, *J. Less Common Met.* 62 (1978) 1.

Received 10 May 1982
and accepted 17 January 1983